Brownian Adhesive Dynamics (BRAD) for Simulating the Receptor-Mediated Binding of Viruses

Thomas J. English* and Daniel A. Hammer[†]

*Department of Chemical and Biomolecular Engineering and [†]Department of Bioengineering, University of Pennsylvania, Philadelphia, Pennsylvania

ABSTRACT   Current viral docking models have relied upon the assumption that bond formation and breakage are independent of viral and docking surface geometry, as well as the forces exerted on the bonds. This assumption, known as the equivalent site hypothesis (ESH), is examined in detail using a newly developed simulation technique—Brownian adhesive dynamics (BRAD). The simulation couples the thermal motion of viral particles with adhesive dynamics models to characterize the effect of bonding on viral motion. We use the binding of HIV-like particles to CD4 expressing cells as a model system to illustrate the utility of BRAD. Comparison of the transition rates between bound states predicted by ESH and the rates resulting from BRAD simulations show dramatic differences; at values of the equilibrium crosslinking constant, $K_x R_T$, where ESH suggests all virus adhesion proteins will be bound ($K_x R_T = 10^6$), BRAD predicts not all virus adhesion proteins will be bound. At values of the equilibrium crosslinking constant used in typical ESH calculations of virus docking ($K_x R_T = 1$) we find BRAD simulations predict no binding. The mean bond density from BRAD models is often much lower than that predicted by ESH for equivalent parameter values. BRAD suggests that the viruses are much less well bound than ESH predicts. The differences suggest that binding models for viruses need to be reexamined closely. BRAD is a simulation technique that will be useful for quantifying the receptor-mediated binding of a wide variety of viruses to cells.

INTRODUCTION

HIV infection remains a significant problem in the world. In 2001, 40 million people were infected with the virus, and 3 million died from complications related to the infection (Ezzell, 2002). Recent developments in antiviral therapies have yielded significant advances in decreasing the serum viral load in patients. These drugs are capable of slowing production of the virus to a point where the immune system can clear virus from the blood. However, it has recently been learned that not only can the virus surreptitiously hide in CD4 cells and the blood, but it can also remain dormant on the surface of follicular dendritic cells (FDCs) and within macrophages (Finzi and Siliciano, 1998). The virus also uses anatomical compartments such as the central nervous system and the male urogenital tract to avoid antiviral therapies (Pierson et al., 2000). These additional cell types and anatomical compartments serve as reservoirs for the virus. The reservoirs explain the appearance of the rapid rise in blood-borne virus immediately after patients—who previously had immeasurable virus in the blood—are removed from antiviral therapy. This partitioning of the virus into different compartments complicates determining the additional length of drug treatment necessary after a patient has no measurable virus in the blood.

A mechanistic understanding of virus binding would be useful for explaining disease progression—for example, the binding of virus to cells in different compartments. It could also help in determining optimal doses of antiviral drugs—maximizing the inhibition of the virus and minimizing the side effects. A mechanistic model of virus binding would also provide insight into viral production methods by determining the maximum shear rate between virus and cell that would allow for virus binding. This information could then be used in bioreactors that utilize viruses. A maximum stirring rate could be selected that promoted transport of material in the reactor, while not inhibiting—or completely stopping—the infection process.

There are four simple steps in the viral lifecycle, here illustrated with HIV. First, the virus attaches to a host cell. HIV uses the viral glycoprotein gp120 on its envelope to attach to the CD4 protein on cells. Second, the viral genetic material is inserted into the host cell—in the case of HIV this is done through fusion and uncoating at the cell surface. Third, the viral genetic material takes over the operation of the host cell, forcing the host cell to manufacture new virus. Fourth, the cell lyses, releasing newly created virus that repeat the cycle. HIV can also be released from the cell during viral manufacture by budding from the cell's surface (Levine, 1992). When HIV attaches to an FDC, the virus remains dormant on the surface of the cell and endocytosis does not occur (Hlavacek et al., 1999b). Many of the theoretical models have centered on the later viral lifecycles. Reaction models have simulated the third and fourth stages of the viral lifecycle for phage viruses (Endy et al., 2000; You et al., 2002). Given the severity of HIV/AIDS, and the multiple cell lines that HIV can infect, accurate quantitative models of the host specificity and binding of HIV would be

useful for understanding the host tropism of different strains of the viruses. Accurate models of viral docking will provide insight into how viruses partition into different cell types, how infection propagates, and how to prevent transmission of viruses.

Currently there is one dominant model of viral docking. Mass balances are written for the population of virus bound by i receptors. These balances include rate terms that account for a virus forming or breaking bonds. Thus, the model consists of a set of n differential equations, where n corresponds to the maximum number of bonds. There is also an algebraic constraint within the model based upon the fact that the sum of potential binding sites and bound sites on the surface of the cell must sum to the total number of binding sites on the surface of the cell (Perelson, 1981; Wickham et al., 1990; Hlavacek et al., 1999b). By making the approximation that the number of available cellular binding sites is equal to the total number of binding sites, the model is converted to a set of linear ordinary differential equations. In the linear form the model becomes a continuous-time Markov chain. Thus, expected times for dissociation can be calculated. Implicit in this model is the assumption that all binding sites have the same rate of bond formation and breakage. This assumption is known as the equivalent site hypothesis (ESH). Recently, Hlavacek and co-workers (1999a) recognized that binding of some viral attachment proteins might occlude the binding of further free viral attachment proteins and used probability arguments to estimate the size of the effect. However, we postulate that the geometry of the virus, the distribution and length of viral attachment proteins and cell receptors, and the random forces placed on molecules due to Brownian motion of the virus—effects not incorporated in the ESH model—will cause further differences in the rates of bond formation and breakage, which are likely different for each receptor viral attachment protein pair. Hence we suspect the ESH is not strictly valid for virus binding, and a more rigorously detailed method is necessary to accurately simulate viral docking.

Adhesive dynamics simulations are another method of modeling biological attachment. Previously, adhesive dynamic simulations were used to simulate receptor-mediated cell adhesion (Hammer and Apte, 1992; Tees et al., 2001; King and Hammer, 2001). The method employs a combination of deterministic equations of motion for the cell itself and probabilistic bond formation and breakage. The probability of a bond forming is a function of the position of the bonding molecules. Generally, the larger the deviation between the tips of adhesion molecules, the less likely a bond is to form. Once a bond is formed it generates forces on the adhering particle. These forces are calculated by modeling the bonds as Hookean springs. The bonding forces are then summed vectorially with other forces on the particle. These forces may be the result of surrounding fluid flow, interfacial forces (i.e., electrostatic forces), or other body forces acting on the particles. Adhesive dynamic simulations have had substantial success in prediction and replication of experimental results for adhesion of cells and beads on surfaces. More background on adhesive dynamic simulations and their application to leukocyte adhesion can be found in work by Hammer and co-workers (Hammer and Apte, 1992; Tees et al., 2001; King and Hammer, 2001). The adhesive dynamics method is extendable to any sized particle that undergoes adhesion. Here, we apply it to viral adhesion to cell surfaces.

Viruses are nanosized particles, whose dominant source of motion is derived from the thermally driven collisions of the surrounding solution—i.e., the Peclet number, which compares convection to diffusion, is often small. Methods for simulating Brownian motion are well developed. Combining Brownian motion simulations with concepts from adhesive dynamics leads to a novel technique to simulate viral attachment to surfaces. We call this new technique Brownian adhesive dynamics (BRAD). The method is completely general, capable of simulating multiple ligand/receptor pairs between the virus and cell, extendable to any geometry, and to any virus/cell system. In the first step of the algorithm, a cell surface and virus particle are created. Viral attachment proteins and cellular attachment proteins are distributed on their respective surfaces. It is assumed that protein diffusion within the membrane can be neglected. This assumption will be relaxed in future work. The virus then undergoes motion due to thermal collisions. At each step of the virus' motion, each attachment protein pair is evaluated for potential bond formation or breakage. The simulation terminates when the virus moves outside the volume of interest, or the maximum number of simulation steps are taken. For the purpose of this article, the value of BRAD has been demonstrated using kinetic rate data from the gp120/CD4 system. Future work will examine the role of system parameters, such as receptor-ligand binding kinetics, on virus binding.

In this article, the BRAD method will be presented in detail. First a discussion of the techniques used to model Brownian motion will be described, followed by a review of the adhesive dynamics models. A set of model parameters will then be presented. We report the steady-state bond number, the fraction of viruses that bind, the rates of bond formation and breakage, and the effect of altering model parameters, such as receptor density, on virus binding. Where appropriate, we compare the model to ESH. The net effect is that BRAD can be used to calculate the docking of viruses to cell surfaces, and we gain insight into the mechanism of virus docking not possible with previous models.

MODELS

To better understand the comparisons between ESH viral docking models and BRAD, a brief overview of the ESH model is warranted. For more background refer to Perelson (1981), Wickham and co-workers (1990), and Hlavacek and co-workers (1999b). As stated in the Introduction, the ESH model is the result of a mass balance performed on each bonded species, generating a system of first-order differential equations with one algebraic constraint,

$$dB_1/dt = -k_rB_1 - (n-1)k_xRB_1 + 2k_{-x}B_2$$
$$dB_i/dt = (n-i+1)k_xRB_{i-1} - ik_{-x}B_i - (n-i)k_xRB_i$$
$$+ (i+1)k_{-x}B_{i+1} \quad i = 2,\ldots,n-1$$
$$dB_n/dt = k_xRB_{n-1} - nk_{-x}B_n$$
$$R_T = R + \sum_{i=1}^{n} iB_i, \tag{1}$$

where B_i is the surface density of viruses bound with i bonds, R is the surface density of unbound receptor molecule, R_T is the total surface density of receptor molecule, k_x is the single site rate constant for the formation of a bond between the virus and the surface, k_{-x} is the single site rate constant for breakage of a bond between the virus and the surface, k_r is the effective rate constant for detachment of a virus bound by a single receptor, and n is the number of viral bonding molecules on the surface of the virus. If the approximation of $R = R_T$ is made (appropriate in the limit of low virus coverage) the model becomes linear, and a continuous-time Markov chain. The rate of going from a virus with i bonds to $i + 1$ bonds is given by $(n-i)k_xR$. The rate of going from a virus with i bonds to $i - 1$ bonds is given by ik_{-x}. Implicit in this model is the assumption that all binding sites have the same intrinsic rate of bond formation and breakage. A schematic diagram of ESH showing the progression from one bonding state to another is shown in Fig. 1. This form of the model does not include the reattachment rate for viruses that become unbound from the cell, as typically included in ESH models (Hlavacek et al., 2002). However, neglecting the reattachment rate does not affect the results from the ESH model because the rate of bond formation is many times larger than the rate of bond breakage. The rates of bond formation and breakage are often determined by fitting the model to patient viral load data (Hlavacek et al., 2000).

Brownian adhesive dynamics

BRAD is a method to calculate the trajectory of a virus by solving the equations of motion. The three forces incorporated into the momentum balance are Brownian, deterministic, and bonding. Brownian forces are the random forces caused by collisions between the particle and the solution molecules. Deterministic forces are caused by electrostatic repulsion, and hydrodynamic flow. The bonding forces result from the extension or compression of receptor-ligand pairs.

Far-field motion

When the virus particle is solely under the influence of the Brownian forces (there are no adhesive forces), a Brownian motion algorithm developed by Torquato and Kim is used to generate the random walk (1989). Torquato and Kim showed that given a fixed distance to travel, r, a particle experiencing only forces due to thermal motion, will take a random time, δt, to travel the given distance. The cumulative distribution for δt is given by
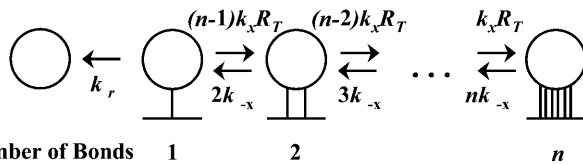

FIGURE 1 Diagram of bond transitions and their associated rates using the ESH model. R_T is the total surface density of receptor molecule, k_x is the single site rate constant for the formation of a bond between the virus and the surface, k_{-x} is the single site rate constant for breakage of a bond between the virus and the surface, k_r is the rate of a singly bound virus dissociating from the cell, and n is the number of viral bonding molecules on the surface of the virus.

$$P(\delta t) = 1 + 2\sum_{m=1}^{\infty}(-1)^m\exp(-Dm^2\pi^2\delta t/r^2), \tag{2}$$

where D is the particle diffusivity, which can be calculated using the Stokes-Einstein relation (Torquato and Kim, 1989). To generate a path taken by such a particle a point is chosen at random on the sphere defined by radius r with the particle initially at the origin. Then $P(\delta t)$ is chosen from a uniform distribution. Eq. 2 can then be solved for δt. To save computation time, the summation in Eq. 2 is truncated at the first term without introducing significant error. This algorithm acts as an adaptive timestep algorithm, and speeds up the calculation by moving the particle a great distance in a single cycle of the algorithm.

Near-field motion

When the viral particle is close to the cell surface, and binding is possible, Brownian motion is calculated using the method of Allen and Tildesley (1987). For a particle experiencing both deterministic and random forces, these differential equations describe the position and velocity of the particle,

$$d\underline{r}/dt = \underline{v}$$
$$d\underline{v}/dt = -\beta\underline{v} + \underline{A} + \underline{K}(\underline{r},t), \tag{3}$$

where r is the vector of positions, v is the vector of velocities, β is the inverse of the viscous relaxation time, A is the vector of accelerations caused by the random forces resulting from thermal motion, and K is the vector of accelerations resulting from deterministic forces caused by bonds or fields acting on the virus (Chandrasekhar, 1943). Electron micrographs of HIV indicate that the virus is spherical (Levine, 1992). Thus, the inverse of the viscous relaxation time can be written as

$$\beta = 3\pi\mu d/m, \tag{4}$$

where μ is the viscosity, d is the diameter of the virus, and m is the mass of the virus. Viruses with different shapes may be simulated with the proper formulation of the drag.

These differential equations can be integrated using an integrating factor. The trajectories can then be generated by evaluating the solutions of the differential equations at specified timesteps δt,

$$\underline{r}(t+\delta t) = \underline{r}(t) + c_1\delta t\underline{v}(t) + c_2\delta t^2\underline{K} + \partial\underline{r}^G$$
$$\underline{v}(t+\delta t) = c_0\underline{v}(t) + c_1\delta t\underline{K} + \partial\underline{v}^G$$
$$c_0 = \exp(-\beta\delta t)$$
$$c_1 = (1-c_0)/(\beta\delta t)$$
$$c_2 = (1-c_1)/(\beta\delta t), \tag{5}$$

where $\partial\underline{r}^G$ is a random position vector and $\partial\underline{v}^G$ is a random velocity vector. The elements of these two random vectors must be chosen in a position velocity pairwise fashion from a bivariate Gaussian distribution. The distribution has a zero mean, and variance and correlation coefficient given by

$$\sigma_r^2 = \delta t^2\frac{k_bT}{m}(\beta\delta t)^{-1}(2 - (\beta\delta t)^{-1}(3 - 4\exp(-\beta\delta t)$$
$$+ \exp(-2\beta\delta t))$$
$$\sigma_v^2 = \frac{k_bT}{m}(1 - \exp(-2\beta\delta t))$$
$$c_{rv}\sigma_r\sigma_v = \delta t\frac{k_bT}{m}(\beta\delta t)^{-1}(1 - \exp(-\beta\delta t))^2. \tag{6}$$

Note that it is assumed that δt is chosen small enough so that the deterministic forces can be approximately constant throughout the timestep. For a detailed derivation of these equations and the distributions from which ∂r^{G} and ∂v^{G} are sampled, see Allen and Tildesley (1987) as well as Chandrasekhar (1943).

In addition to random forces, particles also experience random torques (Berg, 1993). Thus, an additional set of model equations can be written to characterize the angular position and rates of rotation as

$$d\underline{\theta}/dt = \underline{\omega}$$
$$d\underline{\omega}/dt = -\beta_{\text{rot}}\underline{\omega} + \underline{A}_{\text{rot}} + \underline{K}_{\text{rot}}(\underline{r}, t)$$
$$\beta_{\text{rot}} = \pi\mu d^{3}/I, \quad (7)$$

where $\underline{\theta}$ is the vector of angular positions, $\underline{\omega}$ is the vector of angular velocities, A_{rot} is the vector of angular accelerations resulting from random torques to the particle, K_{rot} is the vector of angular accelerations resulting from deterministic torques, β_{rot} is the inverse of the rotational viscous relaxation time, and I is the rotational inertia of the virus. The expressions in Eq. 7 can be solved in exactly the same manner as those in Eq. 3, producing equations analogous to Eq. 5 for calculating the angle and angular rotation of the virus. The variances and correlation coefficients for the rotational motion are given by the expressions in Eq. 6 with I substituted for m and β_{rot} substituted for β.

To model bonding of the virus with the surface, we used the model developed by Dembo et al. (1988). The rate of bond formation and breakage is given as

$$k_{\text{f}} = k_{\text{f}}^{\text{o}}\exp(-(\sigma_{\text{ts}}(x_{\text{m}} - \lambda)^{2})/(2k_{\text{b}}T))$$
$$k_{\text{r}} = k_{\text{r}}^{\text{o}}\exp(((\sigma - \sigma_{\text{ts}})(x_{\text{m}} - \lambda)^{2})/(2k_{\text{b}}T)), \quad (8)$$

where k_{f} is the rate of bond formation, k_{f}^{o} is the standard rate of bond formation, k_{r} is the rate of bond breakage, k_{r}^{o} is the standard rate of bond breakage, σ is the spring constant of the bond, σ_{ts} is the transition state spring constant, x_{m} is the length of the bond, λ is the equilibrium length of the bond, k_{b} is the Boltzmann constant, and T is the temperature. To determine if a bond is formed, first the end-to-end separation distance of the receptor and viral attachment protein is calculated. Then a uniformly distributed random variable is generated. If that number is less than the cumulative probability given by

$$P(\delta t) = 1 - \exp(-k_{\text{f}}\delta t), \quad (9)$$

a bond is formed. To determine if a bond is broken, the length of the bond is calculated, and a uniformly distributed random variable is generated. Then if that number is less than the cumulative probability given by

$$P(\delta t) = 1 - \exp(-k_{\text{r}}\delta t), \quad (10)$$

the bond is broken. It is assumed that all bonding events only occur at the end of each timestep (King and Hammer, 2001; Tees et al., 2001). At the beginning of a timestep, each unbound molecular pair is examined to see if a bond is formed. Also, each bound molecular pair is examined to see if the bond breaks. Forces on the particle resulting from the bonds are calculated by using Hooke's law and are assumed constant throughout the timestep. These forces are then vectorially added into the sum of forces that result in the deterministic acceleration, K, found in Eq. 5.

The virus is prevented from moving through the cell surface by a nonspecific electrosteric force, which is phenomenologically given as $F_{\text{rep}} = 1.5 \times 10^{-27} \, \text{s}^{-1.95}$ N, with the separation distance between the virus and surface, s, given in meters. Similar phenomenological forms have been proposed previously for cell contact phenomena (Bell et al., 1984) and also implemented in adhesive dynamics (King and Hammer, 2001).

The diffusivity of proteins within a membrane is of order $10^{-10} \, \text{cm}^{2}$ per s (Bell, 1978). A bond length is $\sim 10^{-8}$ m. Thus the timescale over which diffusion of proteins within the membrane would be significant would be given by

$$\frac{l^{2}}{D} \approx \frac{(10^{-8}\text{m})^{2}}{10^{-14}\text{m}^{2}/\text{s}} \approx 0.01 \text{ s}. \quad (11)$$

After the initial bond has formed, the simulations will show that steady state between the virus and the cell has occurred well before 0.01 s has elapsed. Thus it is valid to simplify the model by not including protein diffusion throughout the membranes. Therefore, the diffusivity of both gp120 and CD4 within the viral and cellular membranes, respectively, is set equal to zero in these simulations. This fixes the positions of the proteins within their membranes. Immobilizing receptors neglects their lateral motion due to forces acting on molecules, which would drag them through the membrane—this will be corrected in a future version of BRAD. For the purpose of this study, the cell surface is approximated as a plane. This is a reasonable approximation because the diameter of the cell is orders-of-magnitude larger than the diameter of the virus.

A flowchart describing the overall structure of BRAD simulations is shown in Fig. 2. First a virus particle and cell surface is created. This is done by uniformly distributing viral attachment proteins on the surface of the virus, and uniformly distributing receptors on the cell surface. For both the virus and cell surfaces the positions of the proteins are determined by sampling a uniform random distribution. The positions of the proteins are fixed on both the viral and cell surfaces after being generated. At the beginning of each timestep, each bonding molecule pair is examined to determine if a bond is formed or broken. If a bond exists or if the virus is experiencing a deterministic force, such as electrostatic repulsion, the forces from all sources are vectorially summed, and the net displacement in position and velocity is calculated. If the virus is unbound and only under the influence of thermal forces, the maximum distance that the particle can move before it encounters a bonding molecule or a region of deterministic forces is calculated. Then the algorithm, Quickdiff (short for *Quick Diffusion*
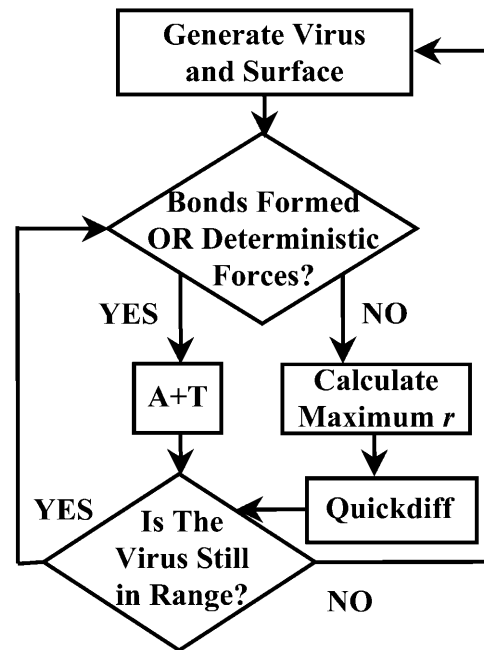

FIGURE 2 Flowchart describing the overall structure of BRAD simulations.

Algorithm), based on the work of Torquato and Kim, is used to update the positions and velocities of the virus. At the end of each timestep, the virus is examined to see if it has moved out of the volume of interest. For the purpose of this article the volume is a cube ~35 viral diameters along each edge, with the cell surface positioned at the base of the cube. If the virus has moved outside of the volume of interest a new virus and cell surface are generated. Otherwise, bonding pairs are evaluated and the process repeats until a prescribed number of timesteps have been taken.

Fig. 3 is a plot of the diffusivity of an unbound virus as a function of the fraction of simulation steps in which the far-field simulation method (Quickdiff) was used. The solid horizontal line is the theoretical diffusivity of the particle calculated by the Stokes-Einstein relationship. The plot shows that the simulated diffusivity agrees with the theoretical diffusivity when up to 90% of the simulation steps are calculated via Quickdiff. Only when all of the steps are calculated via Quickdiff does the simulated diffusivity differ somewhat from theory, though the error is <5%. Therefore, we conclude that the algorithm accurately reproduces the proper Brownian motion of the virus, even when a far-field method is used to calculate the virus motion.

A typical trajectory for the virus center in the vicinity of the cell surface is shown in Fig. 4. Fig. 4 *a* is a diagram of the coordinate system used for the simulations. In Fig. 4 *b* the position of the particle in the *xy* plane in shown. The virus starts with its center at the origin. Note the section of the random walk that appears as a long straight line. The line is the result of a dilated timestep cycle of the algorithm (far-field motion). Fig. 4 *c* is a plot of the *z* position as a function of time. The dotted horizontal line in Fig. 4 *c* represents the *z* position of the center of the virus where the surface of the virus would contact the cell surface. Fig. 4 *d* is a plot of bond number as a function of time. Clearly, as bonding increases, the thermally driven motion of the virus becomes less pronounced, and the separation between virus and surface approaches the equilibrium bond length.

Model parameters

In this article, we will use a model virus similar to HIV to illustrate the value of BRAD. Kinetic rates of CD4/gp120 binding will be used. A difference between HIV structure and the model virus used here is that gp120 is trimerized on an actual HIV particle, which will lead to steric effects and mechanistic details not yet incorporated in the model. Yet, the model is illustrative of the basic principles of virus binding.

A mature HIV is 80–100 nm in diameter, with 8-nm projections of exposed gp41 and gp120 on its surface (Murphy et al., 1995). The simulation results presented in this article use a viral diameter of 90 nm. The

length of gp120 and CD4 is ~5 nm and 6.3 nm, respectively (Kwong et al., 1998). In the simulation the lengths of CD4/gp120, including the portion of exposed gp41 and the unstressed bond, are set at 6.3 nm, 8 nm, and 14.3 nm, respectively. Values of 72–100 groups of gp120 on the surface of the virus have been reported (Murphy et al., 1995; Hlavacek et al., 1999b; Kuznetsov et al., 2003). Simulations presented in this article used a value of 72 groups of gp120 on the surface of its protein envelope. Using scaling arguments and comparison with values from prior adhesive dynamics work, the values of σ and σ_{ts} were set at 1.2×10^{-2} and 3.5×10^{-3} N/m (Chang and Hammer, 2000). Using experimental data from Dimitrov and co-workers, a physiological surface density of CD4 is estimated at 6.3×10^{11} molecules per square centimeter (Dimitrov et al., 1992).

To determine k_f^o and k_r^o for individual bonds we used the kinetic data from Dimitrov and co-workers. Macroscopic kinetic bond formation, k_a, was measured to be $(1.5 \pm 0.42) \times 10^5$ M^{-1} s^{-1}, and macroscopic bond dissociation, k_d, is given as 3.3×10^{-4} s^{-1} at 37°C. In the Dimitrov experiment, gp120 is expressed on the surface of infected cells, then solubilized CD4 is introduced and the binding of CD4 to the gp120 is observed using flow cytometry. The information given by k_a and k_d provides three-dimensional rate information, i.e., including the rate of transport in the bulk solution. However, the rates required by the ESH model and BRAD are two-dimensional, excluding the effect of transport in the bulk solution. It is then necessary to use some method of conversion to transform the experimentally observed rates of Dimitrov into rates of appropriate dimension for the models.

A method presented by Bell can be used to estimate individual bonding rates from the volumetric rate data (Bell, 1978). First the diffusion-limited rate of formation, d_+, and dissolution, d_-, of the encounter complex are calculated as

$$d_+ = 4\pi D_{sCD4} R_{AB}$$
$$d_- = 3 D_{sCD4}/R_{AB}^2, \tag{12}$$

where D_{sCD4} is the diffusivity of soluble CD4 and R_{AB} is the encounter distance for the gp120 and CD4 system. Thus, using the Stokes-Einstein relation, the diffusion coefficient of solubilized CD4 $\approx 8.5 \times 10^{-11}$ m^2 per s and the diffusion coefficient of gp120 will be much smaller than that of the solubilized CD4 because it is fixed to the cell surface in the Dimitrov experiment. The value for the encounter distance was taken as 0.75 nm, the same distance that Bell proposes for the hapten-antibody system. The individual bond formation and breakage rates are then found, solving the following system of equations:
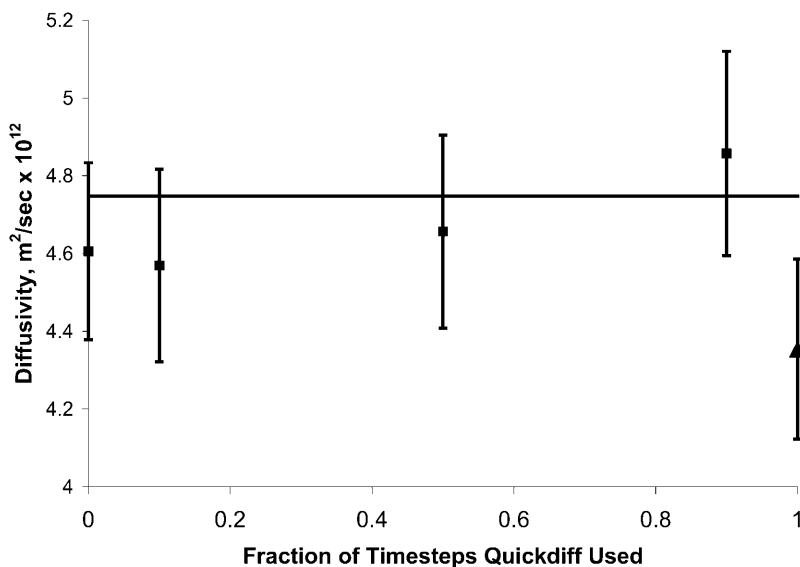

FIGURE 3 Diffusion coefficient calculated from simulation results, ■, as a function of the fraction of the trajectory simulated using the far-field approximation. The solid line depicts the theoretical diffusion coefficient calculated using the Stokes-Einstein relation. The error bars depict the 95% confidence interval. The point represented by a ▲ shows the small error introduced by truncating the summation of Eq. 5 at the first term.
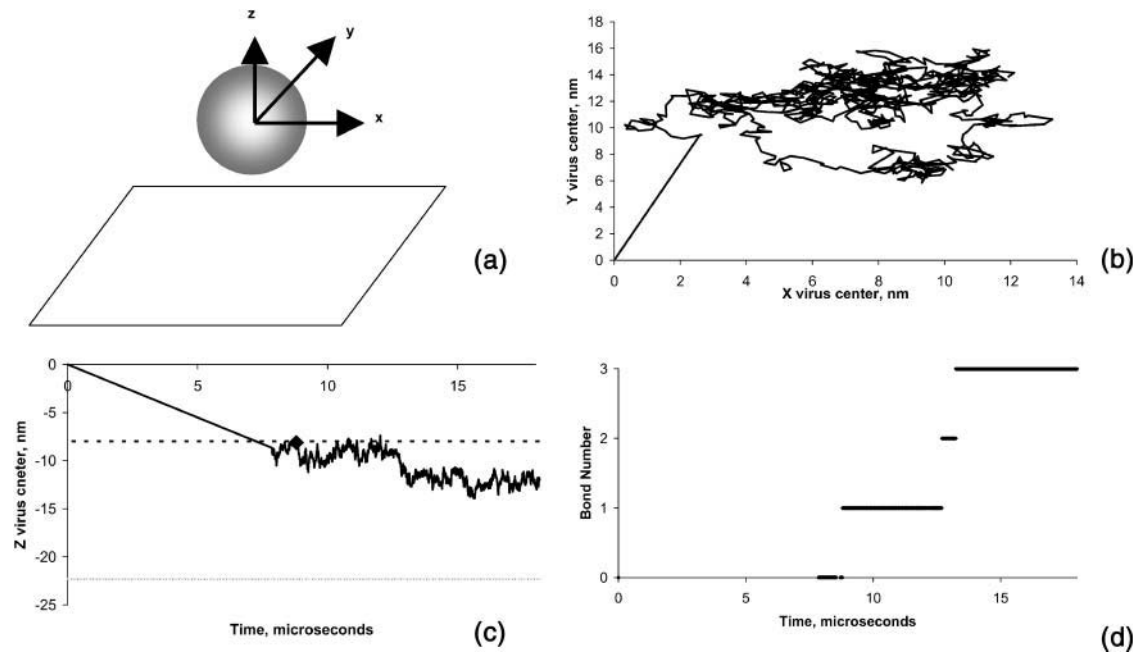
FIGURE 4   Typical trajectory resulting from BRAD simulation. Frame *a* is a diagram of the coordinate system used in BRAD simulations. In *b* the path of the particle in the *xy* plane is displayed. The particle begins at the origin. The straight line segments in the path are a result of the algorithm taking an adaptive timestep cycle. In *c*, the *z* position as a function of time is plotted. The dotted horizontal line indicates the point where the surface of the virus touches the surface of the cell. The dashed line is the center position for the virus when the surface of the virus is one unstressed bond length from the surface of the cell. A diamond indicates the time and *z* position where bonding begins. In *d* the number of bonds as a function of time are plotted. Note that the virus need not touch the surface to form a bond.

$$k_{a} = d_{+} k_{f}^{obs}/(d_{-} + k_{f}^{obs})$$
$$k_{d} = d_{-} k_{r}^{obs}/(d_{-} + k_{f}^{obs}), \qquad (13)$$

where k_{f}^{obs} and k_{r}^{obs} are the intrinsic rates of bond formation and breakage. Using this method, $k_{f}^{obs} \approx 1.4 \times 10^{5}/s$ and $k_{r}^{obs} \approx 3 \times 10^{-4}/s$. It is interesting to note that Myszka et al. (2000) report the free energy of binding between gp120 and CD4 as −11.8 ± 0.3 kcal/mol. This translates to a k_{f}/k_{r} value of 2.0×10^{8} which is within an order of magnitude of that estimated by Dimitrov of 4.6×10^{9}. With large negative values of free energy and large equilibrium constants, bond formation is heavily favored over bond breakage at equilibrium. The intrinsic rates of bond formation and breakage in the Dembo bonding model, k_{f}^{o} and k_{r}^{o}, are set equal to k_{f}^{obs} and k_{r}^{obs}, respectively, for the BRAD simulations.

To make comparisons between BRAD simulations and ESH models the value of k_{x} and k_{-x} must be determined. The two-dimensional rates of the ESH model are found by converting the three-dimensional rates observed in the Dimitrov experiment into two-dimensional rates using the method of Bell (1978). The ESH rates are found using Eq. 13; however, d_{-} and d_{+} are given by Eq. 14 as

$$d_{+}^{m} = 2\pi[D_{m}(CD4) + D_{m}(gp120)]$$

$$d_{-}^{m} = 2[D_{m}(CD4) + D_{m}(gp120)]R_{AB}^{-2}, \qquad (14)$$

where $D_{m}(CD4)$ and $D_{m}(gp120)$ are the membrane diffusivities of CD4 and gp120, respectively. The value of the membrane diffusivities are both taken as $10^{-10} cm^{2}/s$. The ESH model values are then $8.6 \times 10^{-14} m^{2}$ per s and 4.7×10^{-4} s for k_{x} and k_{-x}, respectively. These rates were used to make comparisons to BRAD simulation results with the ESH model. These values of k_{x} and k_{-x} result in a large value for the equilibrium crosslinking constant, $(k_{x}R_{T}/k_{-x} = K_{x}R_{T} = 10^{6}$ where K_{x} is the dimensional crosslinking constant). Hlavacek and co-workers used patient viral load data to set the value of k_{x} and k_{-x} for the FDC/HIV system, which employs different binding proteins. They found the equilibrium crosslinking constant needed to match viral load data was of order one (Hlavacek et al., 1999b). Hlavacek and co-workers examined a range of values for *n* from 10 to 100. To make a fair comparison between ESH and BRAD, the maximum number of observed bonds in all BRAD simulations in this article, 21, was taken as the value of *n*.

Because the value of $K_{x}R_{T}$ is larger than is typically used in viral simulations, such as used by Hlavacek and co-workers, we examined other methods for determining $K_{x}R_{T}$. An alternative, perhaps superior method for determining $K_{x}R_{T}$ comes from the models of crosslinking of multivalent antigens by cell surface immunoglobulins in immune cells (Crothers and Metzger, 1972; Dembo and Goldstein, 1978; Goldstein and Wofsy, 1994). The most lucid of the treatments in that of Goldstein and Wofsy (the other methods yield approximately the same result). In Goldstein and Wofsy, the relationship between K_{x} and K is given, $K_{x} = K/d$, where *d* is the antigen-antigen separation distance. Given the number of viral attachment proteins – 72 – and the area of the virus (based on a 90 nm radius), we estimate $d = 4 \times 10^{-6}$ cm. Based on the direct 3D measurement of $K = 4.55 \times 10^{8} M^{-1} = 8 \times 10^{-13} cm^{3}$ by Dimitrov (given in our article), $K_{x} = 2.1 \times 10^{-7} cm^{2}$, and $K_{x}R_{T} = 1.3 \times 10^{5}$ (based on $R_{T} = 6.3 \times 10^{11} mol/cm^{2}$). Thus, $K_{x}R_{T}$ is still quite large. Calculations performed with this high value of $K_{x}R_{T}$, using the ESH model, in which $k_{x} = 9.7 \times 10^{-11} cm^{2}$ per s, and $k_{-x} = 4.7 \times 10^{-4}$ s give no detectable difference in the steady-state binding of the virus with the cell (since $K_{x}R_{T}$ is so large) and very little difference in the dynamics of approach to steady state. Thus, regardless of what precise model is used to calculate $K_{x}R_{T}$, our basic conclusions regarding the differences between the BRAD and ESH models will be the same.

The viscous relaxation time, $m/3\pi\mu d$, is the time constant for the decay of the acceleration transient caused by collisions between the solution molecules and the particle. As long as the timestep of the difference equations is larger than the viscous relaxation time, it can be assumed that the particle has no inertia. Thus, in BRAD simulations, when the particle is under the influence of deterministic forces there is an upper bound to the timestep, resulting from the desire to have several bonding events per timestep as well as keeping the deterministic forces constant throughout the

step, and a lower bound, set by the viscous relaxation time. For HIV particles a 1-ns timestep satisfies both constraints.

RESULTS

Fig. 5 contains six snapshots of viral positions and bonds during an encounter with the cell surface from BRAD
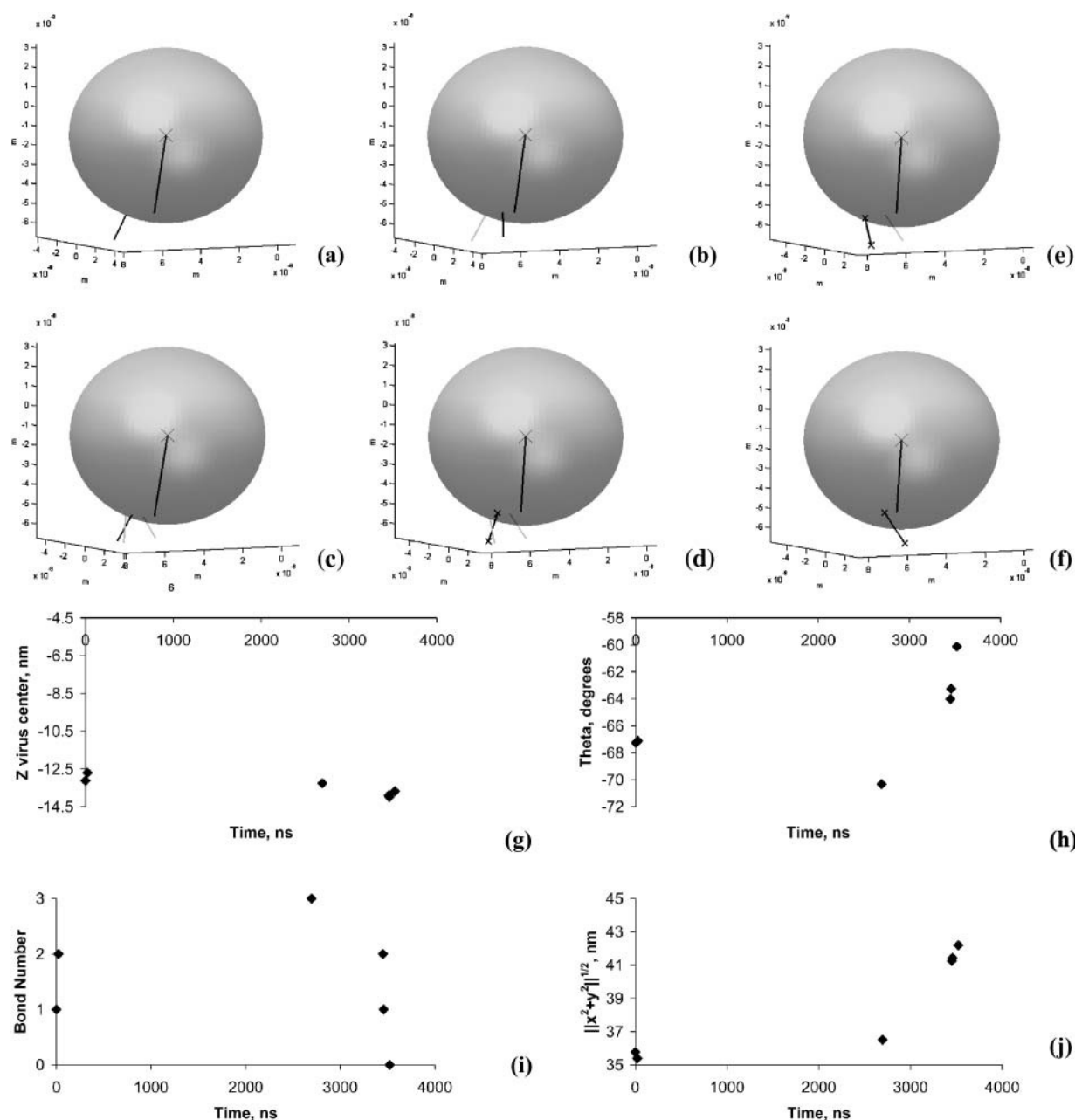

FIGURE 5 Snapshots of viral position and bonds for a transiently adhering virus. Bonds depicted as black lines indicate that the bond was formed in that frame. Bonds depicted as gray lines indicate that the bond had formed before that frame and existed through the frame. Bonds depicted as black lines with an x at the endpoints indicate that the bond was broken in that frame. In this sequence the virus forms bonds with the cell but breaks those bonds and diffuses from the surface. Times for a–f are 0, 22, 2696, 3450, 3458, and 3521 ns, respectively. The bond formation lengths for a–c are 14.4, 16.4, and 15.1 nm, respectively. The bond breakage lengths for d–f are 19.4, 19.9, and 19.3 nm, respectively. Frame g depicts the position of the virus center in the z direction (normal to the cell surface) at the six times depicted in a–f. Frame h is a plot of the angle between the reference vector and the xy plane for each of the times depicted in frames a–f. Frames i and j are plots of bond number and the magnitude of the displacement of the virus center on the xy plane, respectively.
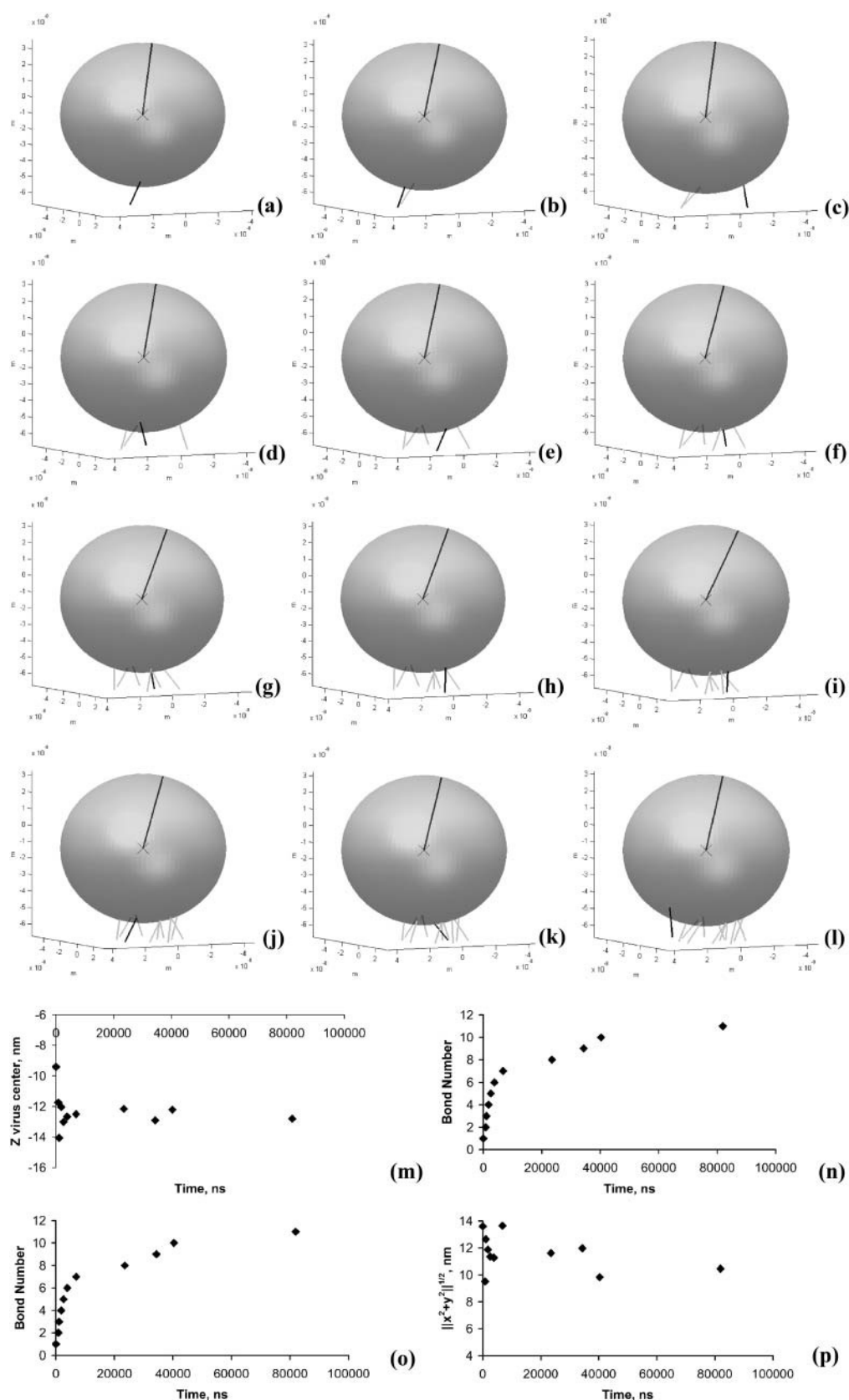
FIGURE 6 Snapshots of viral position and bonds for a transiently adhering virus. Bonds depicted as black lines indicate that the bond was formed in that frame. Bonds depicted as gray lines indicate that the bond had formed before that frame and existed through the frame. In this sequence the virus forms a permanent set of bonds with the cell. Times for frames *a–l* are 0, 789, 1044, 1765, 2544, 3808, 6865, 23,520, 34,341, 40,333, 41,593, and 3,437,903 ns, respectively. The bond formation lengths for *a–l* are 16.0, 14.7, 14.1, 14.9, 14.4, 15.1, 14.2, 15.7, 14.9, 17.0, 16.0, and 18.3 nm, respectively. Frame *m* depicts the position of the virus center in the *z* direction (normal to the cell surface) at the 11 times depicted in *a–k*. Frame *n* is a plot of the angle between the reference vector and the *xy* plane for each of the times depicted in *a–k*. Frames *o* and *p* are plots of bond number and the magnitude of the displacement of the virus center on the *xy* plane, respectively.

simulations in which the virus binds then unbinds from the cell. This simulation employs the physiological cellular receptor density (6.3×10^{11} mol/cm^2). Black lines indicate that the bond was formed in that frame. Black lines with an x at the endpoints indicate that the bond will break immediately following that frame. Gray lines indicate that the bond previously existed. The black line within the sphere is a reference vector to indicate the angular position of the virus. Fig. 5 shows that the virus shuffles back and forth on the surface of the cell while rotating. In this realization, the virus docks and undocks from a cell in a short time. A second simulation performed under the exact same conditions shows a virus that docks irreversibly (Fig. 6). Fig. 5, g–j, and Fig. 6, m–p, illustrate how the virus-cell separation, virus angle, bond number, and displacement in the xy plane change with time for each of the two trajectories.

Fig. 7 is a plot of the bond number as a function of time for five viruses simulated by BRAD, and the predicted mean bond number from the ESH model (*smooth black line*). The dotted lines denote the range in bond numbers that have at least 5% of the total virus surface density according to the ESH model. Fig. 7 a shows the trajectories of several viruses simulated with BRAD and the ESH model up to the time steady state is reached for the simulated viruses. The time shown to reach a steady-state bond number is actually less than the time required in vivo, since the simulations start with the viruses in molecular contact and the ESH calculations are performed with an initial condition of $B_1 = 1$, $B_i = 0$ for $i \neq 1$. Two differences between ESH and BRAD predictions are illustrated in this figure. First, BRAD shows a wider diversity in bond number along the path to steady state than does the ESH model. Second, BRAD predicts a variety of steady-state bond numbers, whereas at sufficiently long times, ESH would predict one steady-state bond number, owing to the high value of $K_x R_T$.

Fig. 8 is a plot of the distribution of steady-state bond number for both BRAD and ESH models using a physiological cellular receptor density. Ninety viruses were simulated to produce the results shown. Of these 90 viruses, 74 formed permanent bonds with the cell instead of diffusing away from
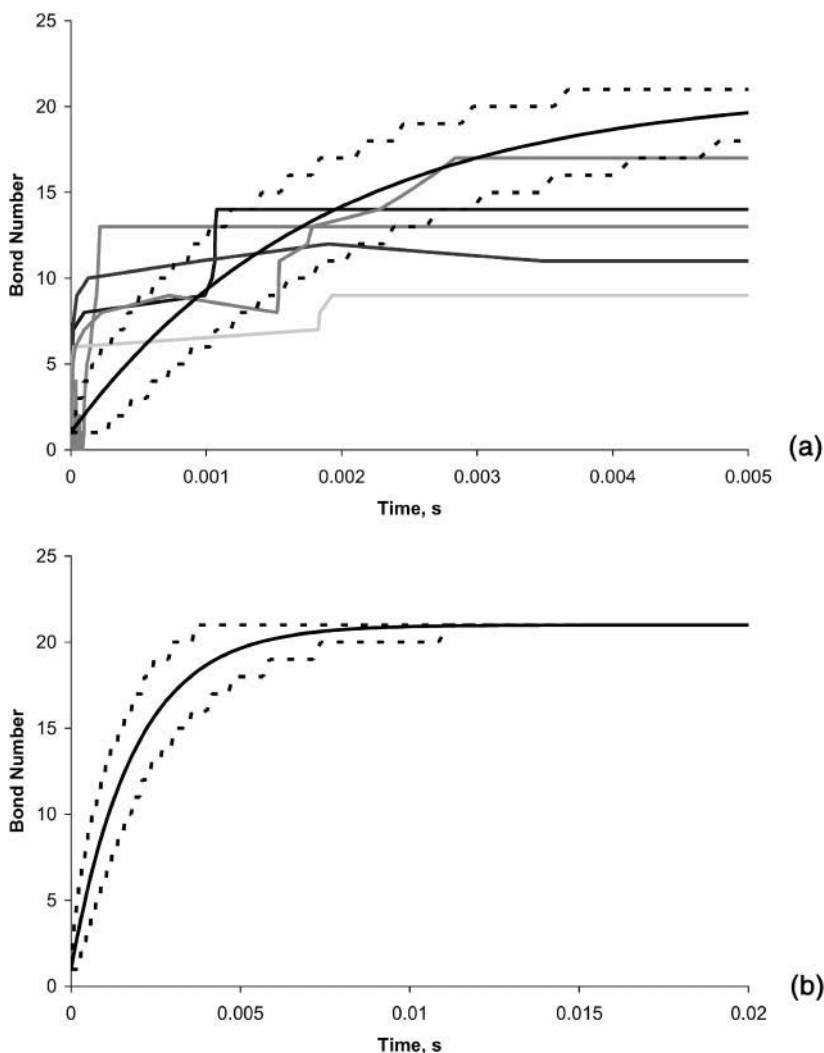

FIGURE 7 Bond number as a function of time for the ESH model, and five examples from BRAD simulations. The ESH model trajectory is shown with a smooth solid black line. The dotted lines denote the minimum and maximum bond numbers that have at least a 5% of the total surface density in the ESH model. (*a*) The ESH model predicts a monotonically increasing transition in mean bond number from one bond to the steady-state value of 21. Frame *b* shows the complete transition to steady state for the ESH model, as well as the collapse of the bond number distribution at steady state. The BRAD trajectories show periods of rapid bond formation followed by periods of inactivity, as well as points at which bonds break. Each BRAD trajectory is different not only in the path to steady state but in steady-state bond number as well. For all trajectories, $t = 0$ at the time when the first bond was formed. Thus, the plot does not show any effect of diffusing in the bulk solution.
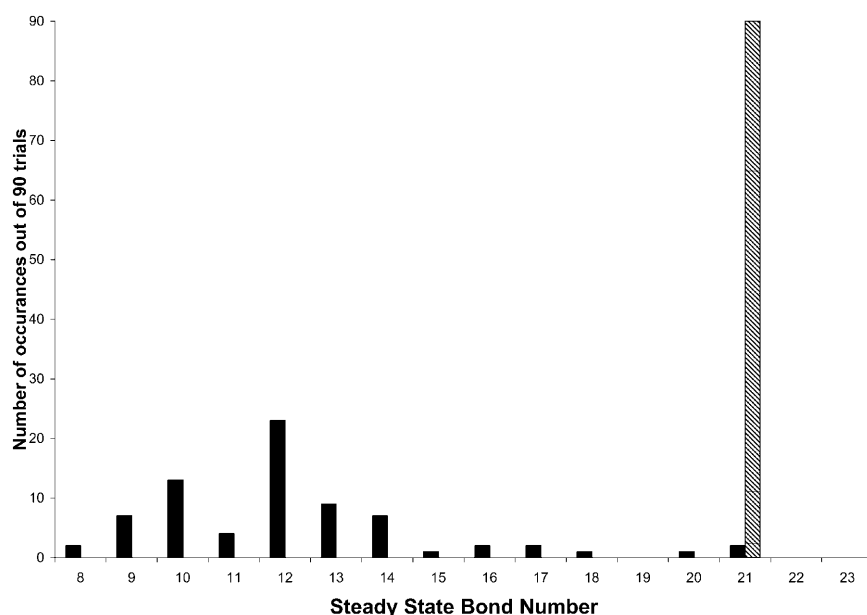
FIGURE 8 Distribution of steady-state bond number using physiological model parameters for both the ESH model and BRAD simulations. The ESH model result is depicted with the hashed bar. All 90 ESH viruses bind to the same steady-state bond number of 21. Sixteen of the ninety BRAD viruses diffused away from the surface before reaching a steady-state bond number with the cell. The remaining 74 BRAD viruses formed a distribution of steady-state bond numbers with the cell.

the surface; the other 16 interacted transiently with the surface, but did not form permanent connections. ESH predicts that all viruses that form one bond with the cell will form permanent bonds with the cell. Furthermore, ESH predicts that all viruses will have the same steady-state number of bonds—n, specifically 21—owing to the large value of $K_x R_T$. BRAD shows a distribution of steady-state bond number with a mean of 12.2 bonds. At steady state, the virus is less well bound, on average, than predicted by ESH.

For $K_x R_T = 10^6$, ESH predicts that all available molecules will bind. Although ESH normally produces a distribution of bond numbers at steady state (i.e., when $K_x R_T = 1$), the overwhelming driving force for binding causes viruses to be fully bound. The value of n is arbitrarily set. One can reason that n should be the maximum number of molecules to possibly bind, which is ~21. Thus, BRAD predicts the virus is much less well bound at steady state for equal parameters. A series of BRAD simulations were run with $K_x R_T = 1$—a value used by Hlavacek and co-workers to match viral

binding data. The intrinsic forward and reverse rates, k_f^o and k_r^o, were both set to 0.1 s. None of the simulated viruses formed a bond with the cell with $K_x R_T = 1$.

Fig. 9 illustrates the sensitivity of the steady-state bond distribution to the cellular receptor surface density. BRAD shows that decreasing the cellular receptor density shifts the steady-state bond distribution to lower bond numbers. ESH would predict the same level of binding for all values of R_T; since $K_x R_T \gg 1$, the virus would be fully bound. Fig. 10 shows in BRAD simulations both the mean steady-state bond number and the fraction of viruses that bind to a steady-state number of bonds before diffusing away from the cell drop as the surface density of cellular receptor is decreased. The ESH model predicts that all viruses will form permanent bonds with the surface if just one bond forms for all surface densities examined. The physiological surface density is the highest surface density shown. Halving the surface density (from 6.3×10^{11} mol/cm^2 to 3.2×10^{11} mol/cm^2) has no measurable effect on the fraction of viruses bound in these
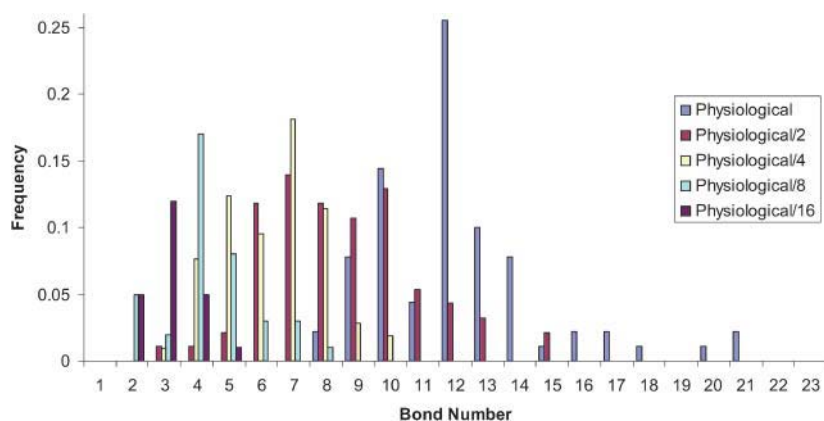

FIGURE 9 Distributions of steady-state bond number for five cellular receptor site densities, calculated with 90 viruses at each density. Decreasing the cellular receptor site density shifts the bond distributions to lower mean numbers.
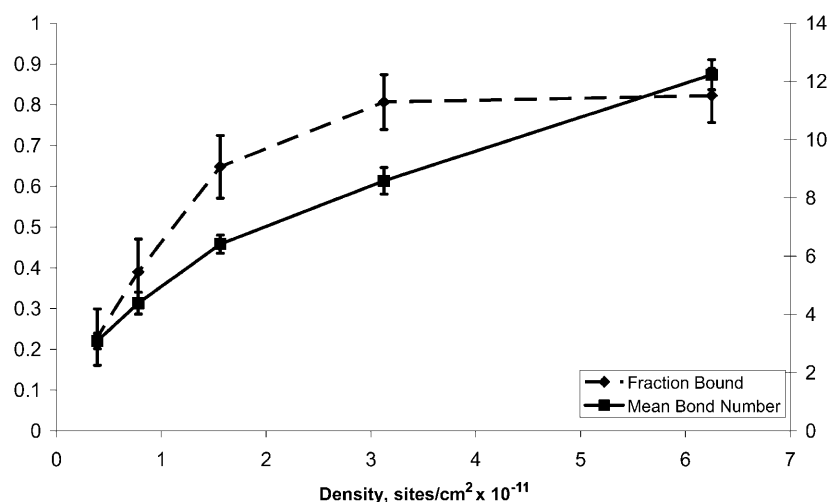
FIGURE 10 Effect of cellular receptor surface density on the mean number of bonds at steady state and the fraction of viruses that permanently bind the cell surface. In each case 90 viruses were simulated using BRAD. Decreasing the physiological cellular receptor surface density by a factor of 2 leaves the fraction of viruses bound unchanged, but decreases the mean bond number. If the density is further reduced a significant decrease in the fraction bound and in the mean bond number is observed. The error bars depict the 90% confidence interval.

simulations. Yet the mean bond number decreases from 12.2 to 8.6. Decreasing the surface density further decreases both the fraction bound and the mean steady-state bond number. The slope of the change in bond density as a function of receptor density increases as the receptor density approaches zero. However, it is not strictly correct to compare the fraction bound between the BRAD simulations and the ESH model. To make a more accurate comparison, it would be necessary to include the rebinding rate in the ESH model, as well as use the probabilistic method of Northrup and co-workers (1984) to extract infinite virus trajectory probabilities from the finite trajectories given by the BRAD simulations.

As a further illustration of the differences between models, we compare the rates of bond breakage. To calculate rates of bond breakage from simulation, the inverse of the time between a bond forming or breaking was taken as the rate. Fig. 11 is a plot of the individual rates of bond breakage for each bond number. There are significant differences between the ESH model and BRAD simulations. First, the rate of bond breakage in the ESH model has no dependence on cellular receptor surface density. In contrast, BRAD

simulations reveal a difference in rates for different cellular receptor surface densities. Second, while the ESH model shows an *increase* in bond breakage rate with increasing bond number (owing to the increased valency of bonds to fail), BRAD simulations show a *decrease* in bond breakage rate with increasing bond number (owing to the fact that the virus is under stress, and the bonds between the virus and surface share the stress, reducing the rate of failure of any one bond).

Effect of σ and σ_{ts} fraction of binding viruses and average bond number

The BRAD algorithm allows us to calculate the effect of spring constants and mechanical properties of virus binding. Fig. 12 shows the effect of varying the bond spring constant, σ, and the transition state spring constant, σ_{ts}, on the fraction of viruses that will bind to the cell before diffusing out of the volume of interest. Two different magnitudes of spring constants are examined: $\sigma_{ts} = 3.5 \times 10^{-3}$N/m and $\sigma = 1.2 \times 10^{-2}$N/m, and a weaker spring set with $\sigma_{ts} = 3.5 \times 10^{-4}$N/m and $\sigma = 1.2 \times 10^{-3}$N/m. Combinations of these
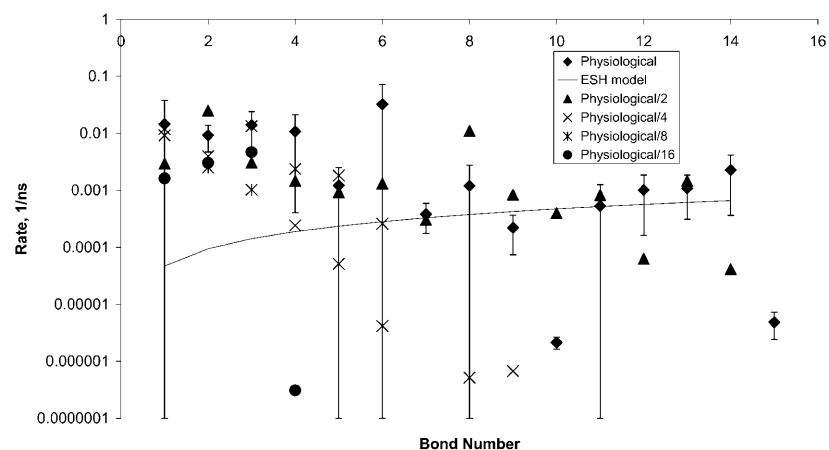

FIGURE 11 Individual rates of bond breakage. The ESH result is represented by the solid black line. The ESH model has no dependence on surface site density for its bond breakage rate. The BRAD simulation results are represented by symbols. Results from calculations using five different cellular receptor surface densities are plotted: physiological, physiological divided by 2, physiological divided by 4, physiological divided by 8, and physiological divided by 16, represented by a ♦, ▲, ×, ✳, and ●, respectively. The 90% confidence interval is depicted only for the physiological receptor density to preserve clarity.
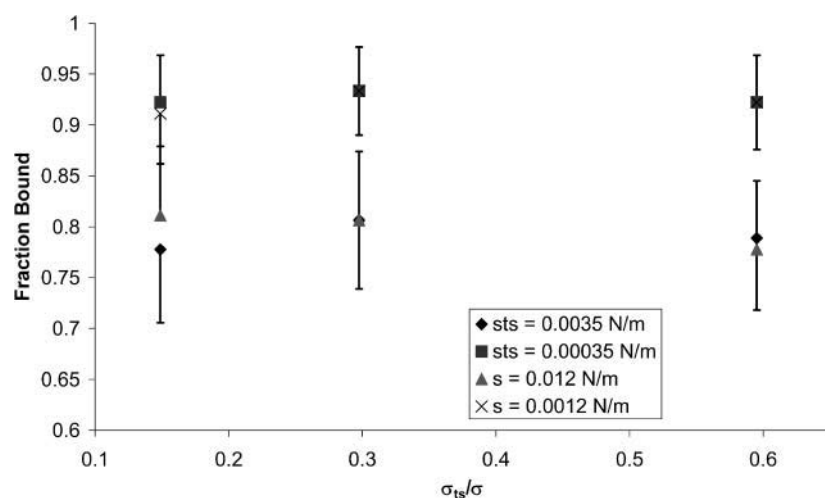
FIGURE 12 The effect of spring constants on the fraction of viruses bound. The fraction bound was determined from simulations using sets of 90 viruses. Results depicted with a ◆, ■, ▲, and × use a σ_{ts} of 3.5×10^{-3} N/m, σ_{ts} of 3.5×10^{-4} N/m, σ of 1.2×10^{-2} N/m, and σ of 1.2×10^{-3} N/m, respectively. Only half of the 90% confidence interval for each point is shown to preserve clarity.

values were also assessed. Changing the ratio of the spring constants has no effect upon the fraction of viruses that bind to steady state. Decreasing both the bond and transition state spring constants, but keeping their ratio constant, increases the fraction of viruses that bind to steady state. However, the decrease in spring constants must be an order of magnitude before a statistically appreciable effect appears. Fig. 13 depicts the effect of altering the spring constants on the average number of bonds at steady state. When the bonds are an order-of-magnitude more compliant, almost twice the number of steady-state bonds is formed at steady state. The increase in fraction bound and the mean bond number for the weaker spring constants is because weaker bonds are capable of acting over larger displacements from the relaxed bond length. Bond number decreases if either the bond or transition state spring constant is increased while the other remains fixed. With the less compliant bonds, a decrease in the transition state spring constant of 50% produced a statistically significant change in bond number—resulting in a 13% increase. Thus, the fraction bound and mean bond number

predictions are not sensitive to the spring constant ratio for less compliant bonds.

CONCLUSION

BRAD simulations are a powerful new tool to determine interactions between viruses and cells. They are capable of providing information on the rate of bond formation and breakage, the fraction of virus/cell collisions that result in permanent binding, the maximum number of bonds between a virus and a cell, and the spatial-temporal organization of bonds in the virus/cell interface. BRAD simulations make several improvements over the traditional ESH model of viral docking. The ESH model assumes all reaction rates are equal. The BRAD model reasons that the rates of reaction will be mechanically controlled by the length of molecules, and the corresponding forces on them. These improvements include the ability to account for the geometry of the virus and cell as well as the positions of the adhesive molecules, to account for the distance-dependent reaction and breakage of
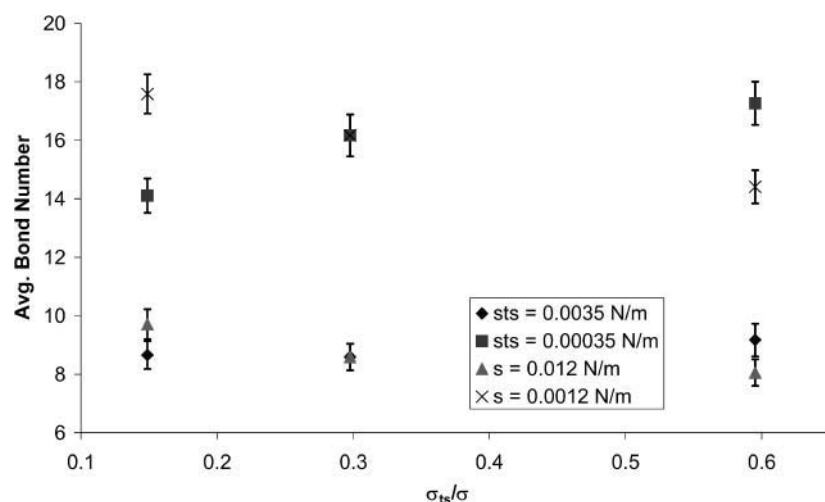

FIGURE 13 The effect of spring constants on the average number of bonds at steady state. The average for each instance was determined from a set of 90 viruses. Results depicted with a ◆, ■, ▲, and × use a σ_{ts} of 3.5×10^{-3} N/m, σ_{ts} of 3.5×10^{-4} N/m, σ of 1.2×10^{-2} N/m, and σ of 1.2×10^{-3} N/m, respectively. The error bars are for the 90% confidence interval.

adhesion molecules, to include the effects of virus thermal motion on bond failure, and to include the effect of molecular mechanics in viral adhesion. These insights may ultimately be very important in calculating the organization of viral attachment protein/receptor complexes in the virus/cell interface during viral docking and fusion.

Comparison of the results of the models for steady-state binding illuminates several differences. At $K_x R_T = \sim 10^6$, all potential binding proteins are predicted to be bound at steady state in ESH. The maximum number of bonds is set by the modeler when choosing a value for the total bond density, based on a reasonable view of the available number of molecules. However, BRAD simulations do not require the artificial selection of the maximum number of bonds that can form. The number of bonds that can form is automatically determined by the algorithm. As such, the simulations show that there is a different steady-state bond number for each receptor density examined. The steady-state number of bonds increases as the receptor density increases, and the steady-state binding is always less than predicted by the ESH model. Thus, it may be that viruses are more weakly bound than previously thought. This is because macroscopic forces are placed on the virus and imparted to the molecules, decreasing bond survival. All of these predictions were made using a value of $K_x R_T = 10^6$. Although this is a much larger value than traditionally used in ESH models, it is in agreement with both thermodynamic and experimentally observed kinetic data for the gp120/CD4 system. When BRAD simulations were run using a traditional value of $K_x R_T = 1$, no viruses bound to the cell surface. Thus, another way to compare the models is that much larger values of $K_x R_T$ are needed in BRAD to achieve the same degree of binding as seen in ESH models; this also suggests binding is weaker than thought.

The rates of molecular interaction predicted by BRAD simulations were compared to rates predicted by ESH. There are significant differences between the simulation rates and the ESH rates. In BRAD, bond breakage rates have a dependence on the surface density of cellular receptor, whereas in the ESH model the rates are independent of surface density. This is because in the BRAD model, multiple bonds share the mechanical load imparted by the virus, making failure much less likely.

The clear value of BRAD is that it provides details of the mechanics of binding and the spatial-temporal organization of receptors in the virus/cell interface. Such detail would be useful in understanding the extent of binding that would precede the fusion of the virus, understanding the relationship between two different bond receptor pairs, and simultaneously exploring the effect of receptor lateral mobility on the organization of receptors in the membrane. This latter effect is easily incorporated by adding a force-dependent lateral motion of the receptor using the known drag of the protein through the lipid (Saffman and Delbruck, 1975; Bussell et al., 1994). Also, many virus proteins such as gp120 exist as trimeric complexes. This trimeric organization can be built into the model. Further, mechanical details of the molecule itself can be added to the model (to understand how viral molecules act as micro machines). Therefore, future work with BRAD will add physical-chemical effect of CD4/gp120 binding, applicable to HIV docking, to develop as accurate a simulation as possible. We suspect such a simulation will be useful for assessing the potency and mechanism of action of pharmaceuticals designed to interfere with viral adhesion and entry.

REFERENCES

Allen, M., and D. Tildesley. 1987. Computer Simulations of Liquids. Oxford University Press, New York.

Bell, G. I. 1978. Models for the specific adhesion of cells to cells. *Science*. 200:618–627.

Bell, G. I., M. Dembo, and P. Bongrand. 1984. Cell adhesion competition between nonspecific repulsion and specific bonding. *Biophys. J.* 45:1051–1064.

Berg, H. C. 1993. Random Walks in Biology. Princeton University Press, New Jersey.

Bussell, S. J., D. A. Hammer, and D. L. Koch. 1994. The effect of hydrodynamic interactions on the tracer and gradient diffusion of integral membrane-proteins in lipid bilayers. *J. Fluid Mech.* 258:167–190.

Chandrasekhar, S. 1943. Stochastic problems in physics and astronomy. *Rev. Mod. Phys.* 15:4–91.

Chang, K. C., and D. A. Hammer. 2000. Adhesive dynamics simulations of Sialyl-Lewis$_x$/E-selectin-mediated rolling in a cell-free system. *Biophys. J.* 79:1891–1902.

Crothers, D. M., and H. Metzger. 1972. The influence of polyvalence on the binding properties of antibodies. *Immunochemistry*. 11:341–357.

Dembo, M., and B. Goldstein. 1978. Theory of equilibrium binding of symmetric bivalent haptens to cell surface antibody: application to histamine release from basophils. *J. Immunol.* 121:345–353.

Dembo, M., D. C. Torney, K. Saxman, and D. Hammer. 1988. The reaction-limited kinetics of membrane-to-surface adhesion and detachment. *Proc. R. Soc. Lond. B Biol. Sci.* 234:55–83.

Dimitrov, D. S., K. Hillman, J. Manischewitz, R. Blumenthal, and H. Golding. 1992. Kinetics of soluble CD4 binding to cells expressing human immunodeficiency virus type 1 envelope glycoprotein. *J. Virol.* 66:132–138.

Endy, D., L. You, J. Yin, and I. J. Molineux. 2000. Computation, prediction, and experimental tests of fitness for bacteriophage T7 mutants with permuted genomes. *Proc. Natl. Acad. Sci. USA*. 97:5375–5380.

Ezzell, C. 2002. Hope in a vial. *Sci. Am.* 286:38–45.

Finzi, D., and R. F. Siliciano. 1998. Viral dynamics in HIV-1 infection. *Cell*. 93:665–671.

Goldstein, B., and C. Wofsy. 1994. Aggregation of cell receptors. *Lect. Math. Life Sci.* 24:109–135.

Hammer, D. A., and S. M. Apte. 1992. Simulation of cell rolling and adhesion on surfaces in shear flow: general results and analysis of selectin-mediated neutrophil adhesion. *Biophys. J.* 63:35–57.

Hlavacek, W. S., J. K. Percus, O. E. Percus, A. S. Perelson, and C. Wofsy. 2002. Retention of antigen on follicular dendritic cells and B lymphocytes through complement-mediated multivalent ligand-receptor interactions: theory and application to HIV treatment. *Math. Biosci.* 176:185–202.

Hlavacek, W. S., R. G. Posner, and A. S. Perelson. 1999a. Steric effects on multivalent ligand-receptor binding: exclusion of ligand sites by bound cell surface receptors. *Biophys. J.* 76:3031–3043.

Hlavacek, W. S., N. I. Stilianakis, D. W. Notermans, S. A. Danner, and A. S. Perelson. 2000. Influence of follicular dendritic cells on decay of HIV during antiretroviral therapy. *Proc. Natl. Acad. Sci. USA.* 97:10966–10971.

Hlavacek, W. S., C. Wofsy, and A. S. Perelson. 1999b. Dissociation of HIV-1 from follicular dendritic cells during HAART: mathematical analysis. *Proc. Natl. Acad. Sci. USA.* 96:14681–14686.

King, M. R., and D. A. Hammer. 2001. Multiparticle adhesive dynamics. Interactions between stably rolling cells. *Biophys. J.* 81:799–813.

Kuznetsov, Y. G., J. G. Victoria, W. E. Robinson, Jr., and A. McPherson. 2003. Atomic force microscopy investigation of human immunodeficiency virus (HIV) and HIV-infected lymphocytes. *J. Virol.* 77:11896–11909.

Kwong, P. D., R. Wyatt, J. Robinson, R. W. Sweet, J. Sodroski, and W. A. Hendrickson. 1998. Structure of an HIV gp120 envelope glycoprotein in complex with the CD4 receptor and a neutralizing human antibody. *Nature.* 393:648–659.

Levine, A. J. 1992. Viruses. Scientific American Library, New York.

Murphy, F. A., C. M. Fauquet, D. H. L. Bishop, S. A. Ghabrial, A. W. Jarvis, and G. P. Martelli. 1995. Virus Taxonomy: Classification and Nomenclature of Viruses: Sixth Report of the International Committee on Taxonomy of Viruses. Springer-Verlag, New York.

Myszka, D. G., R. W. Sweet, P. Hensley, M. Brigham-Burke, P. D. Kwong, W. A. Hendrickson, R. Wyatt, J. Sodroski, and M. L. Doyle. 2000. Energetics of the HIV gp120–CD4 binding reaction. *Proc. Natl. Acad. Sci. USA.* 97:9026–9031.

Northrup, S. H., S. A. Allison, and J. A. McCammon. 1984. Brownian dynamics simulations of diffusion-influenced bimolecular reactions. *J. Chem. Phys.* 80:1517–1524.

Perelson, A. S. 1981. Receptor clustering on a cell-surface. 3. Theory of receptor cross-linking by multivalent ligands—description by ligand states. *Math. Biosci.* 53:1–39.

Pierson, T., J. McArthur, and R. F. Siliciano. 2000. Reservoirs for HIV-1: mechanisms for viral persistence in the presence of antiviral immune responses and antiretroviral therapy. *Annu. Rev. Immunol.* 18:665–708.

Saffman, P. G., and M. Delbruck. 1975. Brownian motion in biological membranes. *Proc. Natl. Acad. Sci. USA.* 72:3111–3113.

Tees, F. J., J. T. Woodward, and D. A. Hammer. 2001. Reliability theory for receptor-ligand bond dissociation. *J. Chem. Phys.* 114:7483–7496.

Torquato, S., and I. C. Kim. 1989. Efficient simulation technique to compute effective properties of heterogeneous media. *Appl. Phys. Lett.* 55:1847–1849.

Wickham, T. J., R. R. Granados, H. A. Wood, D. A. Hammer, and M. L. Shuler. 1990. General analysis of receptor-mediated viral attachment to cell surfaces. *Biophys. J.* 58:1501–1516.

You, L., P. F. Suthers, and J. Yin. 2002. Effects of *Escherichia coli* physiology on growth of phage T7 in vivo and in silico. *J. Bacteriol.* 184:1888–1894.